Photochemical Studies of $CH_3C(O)OONO_2$ (PAN) and $CH_3CH_2C(O)OONO_2$ (PPN): NO_3 Quantum Yields

Matthew H. Harwood,[†] James M. Roberts, Gregory J. Frost,[†] A. R. Ravishankara,[‡] and James B. Burkholder*

Aeronomy Laboratory, National Oceanic and Atmospheric Administration, 325 Broadway, Boulder, Colorado 80305-3328

Received: July 1, 2002; In Final Form: October 21, 2002

The quantum yields for the production of NO_3 in the gas-phase UV photolysis of peroxyacetyl nitrate (PAN, $CH_3C(O)OONO_2$) and peroxypropionyl nitrate (PPN, $CH_3CH_2C(O)OONO_2$) at 248 and 308 nm were measured. We report room-temperature quantum yield values of 0.19 ± 0.04 and 0.41 ± 0.10 at 248 and 308 nm, respectively, for PAN and 0.22 ± 0.04 and 0.39 ± 0.04 at 248 and 308 nm, respectively, for PPN. UV absorption cross sections for PPN between 200 and 340 nm over the temperature range 296−253 K are also reported. The atmospheric implications of these results are discussed.

1. Introduction

Peroxyacetyl nitrate (PAN, $CH_3C(O)OONO_2$) and peroxypropionyl nitrate (PPN, $CH_3CH_2C(O)OONO_2$) are important components of atmospheric reactive nitrogen, NO_y.[1−3] Peroxyacetyl nitrates are phytotoxic and mutagenic at high concentrations and are, therefore, of societal interest in polluted areas. This class of compounds are often a large fraction of NO_y in the remote troposphere and, hence, are important reservoir species for NO_x ($NO_x = NO + NO_2$). The fraction of NO_y comprised as PAN varies from ∼15% in the polluted continental boundary layer[4] to as much as 80% in the high-latitude upper troposphere.[5] The abundance of PAN in the stratosphere is expected to be much less but has not been well characterized. Results from numerical modeling studies have recently shown that transport of PAN constitutes an important source of NO_x to the remote troposphere[6] and can be important in mediating the concentration of NO_x in the upper troposphere.[7] Atmospheric measurements have also shown that PAN is typically more abundant than PPN with the ratio of PPN to PAN varying from a few percent to over 15% in the troposphere.[8]

PAN is formed in the troposphere as a reaction product in the oxidation of various hydrocarbons (i.e., isoprene and acetone) through the association reaction:

$$CH_3C(O)OO + NO_2 + M \leftrightarrow CH_3C(O)OONO_2 + M \quad (1,-1)$$

PPN is formed following the oxidation of larger, $\geq C_3$, primarily anthropogenic hydrocarbons. The atmospheric loss processes for PAN and PPN include the highly temperature dependent thermal decomposition (−1), UV photolysis, and reaction with the OH radical.[9] Heterogeneous losses of PAN and PPN are expected to be slow.[2] However, Villalta et al.[10] have shown that the heterogeneous loss of the $CH_3C(O)OO$ radical, which could be in equilibrium or steady-state, reaction 1, with PAN, could be important under certain atmospheric conditions. Therefore, a heterogeneous loss of $CH_3C(O)OO$ is thus a loss of PAN. The thermal decomposition loss rates for PAN and PPN are strongly temperature dependent, which translates to a strong altitude dependence. Talukdar et al.[9] have shown the atmospheric lifetime of PAN in the low-temperature regions of the upper troposphere, greater than ∼7 km, to be controlled by photodissociation and to be of the order of weeks to months. The different photolytic pathways possible for PAN (see below) could result in a different impact on the remote atmosphere. The characterization of the atmospheric photolysis rate and quantum yields for PPN has received much less attention than PAN in the literature. Field measurements of the PPN to PAN relative abundance have been used as a diagnostic to characterize biogenic and anthropogenic sources to tropospheric ozone production.[8,11] However, differences in the photochemistry of PAN and PPN need to be accounted for in such an interpretation.

There are a number of PAN and PPN photolysis channels energetically accessible in the wavelength region important in the troposphere, $\lambda > 290$ nm. In a simplified picture, these photolysis channels lead to the production of either NO_2 or NO_3

$$PAN + h\upsilon \rightarrow R + NO_2 \quad (2a)$$

$$\rightarrow R' + NO_3 \quad (2b)$$

where $R = CH_3C(O)OO$ and $R' = CH_3C(O)O$ or energetically allowed fragments of these radicals. For PPN photolysis, $R = CH_3CH_2C(O)OO$ and $R' = CH_3CH_2C(O)O$. Mazely et al.[12,13] have recently reported measurements of the NO_2 and NO_3 quantum yields following pulsed laser photolysis of PAN at 248 nm. NO_2, reaction 2a, was observed to be the dominant photodissociation product with a quantum yield of 0.83 ± 0.09. In their later study, NO_3, reaction 2b, was determined to be a significant photodissociation product with a quantum yield of 0.3 ± 0.1. The production of both NO_2 and NO_3 is an indication that the dynamics of the photodissociation process may involve multiple excited electronic states or is not a simple one-step dissociative process. The extrapolation of the short wavelength, 248 nm, photodissociation results to the wavelength range applicable to atmospheric photolysis, >290 nm, needs to be

* To whom correspondence should be addressed. NOAA, R/AL2, 325 Broadway, Boulder, CO 80305-3328. E-mail: burk@al.noaa.gov.

[†] Also associated with the Cooperative Institute for Research in Environmental Sciences, University of Colorado, Boulder, CO 80309.

[‡] Also associated with the Department of Chemistry and Biochemistry, University of Colorado, Boulder, CO 80309.

10.1021/jp0264230 CCC: $25.00
Published on Web 02/04/2003

evaluated. To date there have been no photodissociation studies of the PPN molecule reported in the literature.

In this work, we report quantum yields for the production of NO_3 in the photolysis of PAN and PPN at 248 and 308 nm. NO_3 was detected by long path transient diode laser absorption at 661.9 nm and was quantified relative to N_2O_5 photolysis. As part of this work, PPN UV absorption cross sections over the wavelength range 210−340 nm between 253 and 296 K were measured using a diode array spectrometer. Our results are compared with the previous PAN quantum yield measurements of Mazely et al.[12,13] and the PPN UV absorption cross sections reported by Senum et al.[14] The atmospheric significance of these results is discussed.

2. Experimental Details

In this study, we have measured the UV absorption cross sections of PPN and the quantum yields for NO_3 production following the pulsed excimer laser photolysis of PAN and PPN at 248 and 308 nm. The room-temperature UV cross sections were measured using a diode array spectrometer and absolute pressure measurements. The temperature dependence of the PPN cross section was measured relative to the room-temperature values. The NO_3 quantum yield measurements were made by photolyzing a known concentration of PAN or PPN (determined by UV absorption spectroscopy) with a pulsed excimer laser and measuring the concentration of NO_3 produced with a tunable diode laser operating at 661.9 nm. The excimer laser fluence was calibrated in separate experiments by photolyzing N_2O_5 and measuring the NO_3 yield by absorption. A description of the apparatus and methods used is presented below.

UV Absorption Measurements. PPN absorption cross section measurements were made using a 30 W D_2 lamp light source coupled to a 1024 element diode array spectrometer. The 0.5 m spectrometer used a 150 grooves per mm grating, ∼1.4 nm resolution, and covered the wavelength range 200−520 nm. The wavelength of the spectrograph was calibrated using emission lines from a Hg pen-ray lamp and was accurate to 0.2 nm. Cross section determinations at wavelengths greater than 300 nm were made using a Pyrex optical filter mounted at the entrance of the spectrometer. The filter reduced scattered light contributions to the weak absorption signals at wavelengths >300 nm. Spectra were recorded by coadding 20−100 detector readings with exposure times between 0.02 and 0.08 s.

Two different absorption cells were used during the course of these experiments. The single pass absorption cells were jacketed for temperature regulation and had optical path lengths of 132 and 200 cm. The cells were made from small diameter glass, i.d. 15 mm, to minimize the volume and quartz windows sealed via O-ring joints. Absorption spectra were determined by first measuring the lamp spectrum $I_0(\lambda)$ with the cell evacuated. Gas-phase PPN was then added to the cell directly from the sample reservoir and another spectrum $I(\lambda)$ recorded. Absorption spectra were calculated using $A(\lambda) = -\ln(I(\lambda)/I_0(\lambda))$ and cross sections determined from plots of $A(\lambda)$ vs [PPN]. The cell pressure was measured using a 10 Torr capacitance manometer. The pressure of PPN in the absorption cell ranged from 0.1 to 1.2 Torr. The gas-phase concentrations of PAN and PPN were observed to be stable over the duration of the absorption and quantum yield measurements. All absolute cross section determinations were performed at room temperature, 296 ± 2 K.

The temperature dependence of the PPN absorption spectrum was determined relative to the room-temperature cross section values. A 25 cm long room-temperature absorption cell was attached in parallel with the diode array absorption cell to enable simultaneous measurements with the same sample. Absorption measurements in the 25 cm cell were made using a Zn lamp (213.9 nm) and a phototube detector with a narrow band-pass filter. Absorption measurements with the Zn lamp were made simultaneously with the diode array measurements. The room-temperature cross section values at 213.9 nm (from the absolute pressure measurements) were then used to normalize the diode array spectra recorded at 273 and 253 K.

Experiments were also performed in which a Fourier transform infrared spectrometer was used to measure the infrared absorption spectrum, 1 cm^{-1} resolution over the range 400−4000 cm^{-1}, of the same PPN gas-phase sample simultaneously with the diode array UV absorption measurements at 296 K. The infrared absorption cell was 2.5 cm diameter glass tubing, 10 cm path length, with KBr windows. The infrared and UV absorption cells were filled from the sample reservoir simultaneously to the same total pressure. The infrared measurements served two purposes: (1) to identify possible sample impurities (i.e. propionic acid ($CH_3CH_2C(O)OH$ and propionic anhydride ($CH_3CH_2C(O)OC(O)CH_2CH_3$)) which would otherwise be difficult to detect in the UV due to the continuous and overlapping nature of the spectra and (2) provide a secondary check of the UV absorption cross section determination by comparison with literature values of the PPN infrared absorption cross sections.[15,16]

The absorption signal due to NO_2 which is present as a small impurity and decomposition product in the PPN sample, typically 4×10^{-3} mole fraction, was subtracted using reference spectra measured under identical conditions. The contribution of NO_2 to the PPN absorption signal was only significant at wavelengths >300 nm. Reference spectra of propionic acid, $CH_3CH_2C(O)OH$, and propionic anhydride, $CH_3CH_2C(O)OC(O)CH_2CH_3$, which are both present in the PPN synthesis, were recorded and were found to make negligible contributions to the measured UV absorption spectra on bases of the infrared measurements of the sample.

NO_3 Quantum Yield Measurements. The apparatus and data analysis used for the quantum yield measurements has been described in detail previously.[17,18] The apparatus consisted of a small volume glass cell (i.d. = 0.9 and 100 cm long) with quartz windows through which gas-phase samples of PAN, PPN, or N_2O_5 diluted in N_2 flowed through. Absorption spectra recorded over the wavelength range 210−365 nm using a D_2 lamp and diode array spectrometer were used to determine the concentrations. Absorption cross section data from previous studies were used to quantify the PAN[9] and N_2O_5[18] concentrations. PPN absorption cross sections were taken from this work.

The pulsed photolysis light sources were KrF (248 nm) and XeCl (308 nm) excimer lasers. The photolysis beam passed through the length of the cell collinearly with the diode laser probe beam. The tunable diode laser (5 mW) nominally operating at 661.9 nm was used to detect the NO_3 photofragment. The tunable diode laser beam was passed through cutoff filters to attenuate the photolysis beam before detection by a red sensitive photodiode. The stability of the tunable diode laser allowed absorbance changes of 5×10^{-5} to be measured (S:N ratio of 1).

Quantum yield and photolysis laser fluence calibration measurements were made by first establishing a stable flow of the photolyte (PAN, PPN, or N_2O_5) through the absorption cell. The photolyte concentration was measured by UV absorption as described above. The diode laser beam intensity was then measured prior to firing the photolysis laser. The photolysis laser

was fired (20 ns pulse width) and the diode laser temporal profile measured over the next 4 ms. NO_3 absorption was calculated using the prephotolysis diode laser beam intensity as I_0. Signal averaging was accomplished by coadding diode laser signals from 10 to 50 laser shots. The photolyte concentration was remeasured following the photolysis measurements to confirm its stability during the photolysis measurements.

The NO_3 produced as a photolysis product of X (X = PAN, PPN, or N_2O_5) under optically thin conditions is given by

$$[NO_3]_X = [X]\sigma_\lambda(X)\Phi_\lambda^{NO_3}(X)F(\lambda) \quad (3)$$

where $F(\lambda)$ is the photolysis laser fluence (photon cm^{-2} $pulse^{-1}$) at wavelength λ, $\sigma_\lambda(X)$ is the absorption cross section of X (cm^2 $molecule^{-1}$) at wavelength λ and $\Phi_\lambda^{NO_3}(X)$ is the NO_3 quantum yield from X at the photolysis wavelength. For each set of quantum yield determinations for PAN and PPN, the photolysis laser fluence was held constant and N_2O_5 was used as the reference compound to determine the laser fluence.

Taking eq 3 with a constant $F(\lambda)$ for X = PAN and N_2O_5 (reference compound) yields the NO_3 quantum yield for PAN written in terms of the measured NO_3 absorption signals and photolyte concentrations as

$$\Phi_\lambda^{NO_3}(PAN) = \frac{A_{NO_3}(PAN)[N_2O_5]\sigma_\lambda(N_2O_5)\Phi_\lambda^{NO_3}(N_2O_5)}{A_{NO_3}(N_2O_5)[PAN]\,\sigma_\lambda(PAN)} \quad (4)$$

A similar expression can be written for the PPN quantum yield.

NO_3 has a strong broad absorption band peaking at 661.9 nm ($\sigma_{max} = 2.23 \times 10^{-17}$ cm^2 $molecule^{-1}$).[19] The tunable diode laser was tuned to the peak of the absorption feature to obtain maximum sensitivity to NO_3. The value of the NO_3 absorption cross section is not required in the analysis as shown in eq 4. The absorption cross sections and quantum yields at the photolysis wavelengths used in the data analysis are taken from Harwood et al.[18] for N_2O_5, Talukdar et al.[9] for PAN and this work for PPN.

Materials. The carrier gas was N_2(UHP). PAN and PPN samples were prepared and stored in tridecane solvent as described by Williams et al.[20] The PAN and PPN gas flow through the cell was controlled by regulating the carrier gas flow over the liquid sample, which was, held at temperatures in the range 269−273 K. N_2O_5 was prepared by the reaction between O_3 and NO_2 and stored at 195 K. N_2O_5 was delivered to the reaction cell by passing the carrier gas over the solid.

Gas flow rates for the photolysis experiments were controlled by stainless steel needle valves and measured by electronic mass flowmeters. The total pressure in the cell was 520 Torr and was measured with a 1000 Torr capacitance manometer. All measurements were made at room temperature, ~296 K.

3. Results and Discussion

PPN UV Absorption Cross Sections. The UV absorption cross sections of PPN were determined at 296, 273, and 253 K. Cross section determinations at temperatures lower than 253 K were not performed due to limitations imposed by the PPN vapor pressure. The measured spectra are shown in Figure 1. The spectra show a wavelength-dependent systematic decrease in absorption cross section with decreasing temperature. The temperature dependence of the cross section values was parametrized to the form

$$\ln[(\sigma(\lambda,T)/\sigma(\lambda,296\text{ K})] = B(\lambda)(T - 296) \quad (5)$$

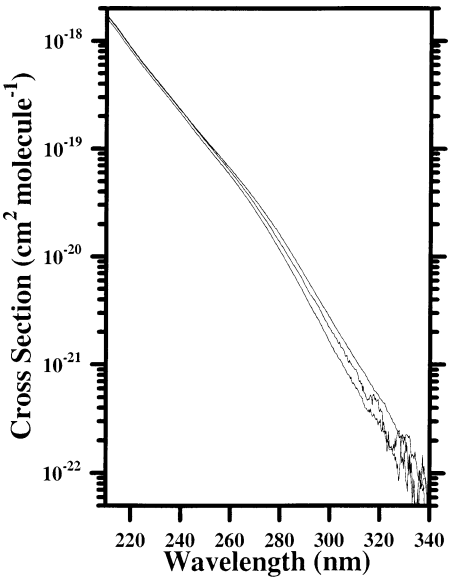

Figure 1. UV absorption cross sections of PPN ($CH_3CH_2C(O)OONO_2$) measured at 296, 273, and 253 K using a diode array spectrometer. The values of $\sigma(\lambda,296\text{ K})$ and $B(\lambda)$ obtained from a least-squares fit of the spectra to $\ln[(\sigma(\lambda,T)/\sigma(\lambda,296\text{ K})] = B(\lambda)(T - 296)$ are given in Table 1.

TABLE 1: UV Absorption Cross Sections and Temperature Coefficients for PPN, $CH_3CH_2C(O)OONO_2$

λ (nm)	σ(296 K)[a]	B[b]	λ (nm)	σ(296 K)[a]	B[b]
210	1.74	1.22	276	0.0214	6.17
212	1.54	1.20	278	0.0184	6.49
214	1.35	1.19	280	0.0157	6.83
216	1.15	1.20	282	0.0133	7.18
218	0.999	1.21	284	0.0112	7.54
220	0.861	1.24	286	0.00940	7.91
222	0.747	1.27	288	0.00790	8.29
224	0.648	1.32	290	0.00662	8.68
226	0.569	1.37	292	0.00551	9.08
228	0.496	1.44	294	0.00462	9.49
230	0.436	1.52	296	0.00389	9.91
232	0.383	1.60	298	0.00325	10.3
234	0.336	1.70	300	0.00273	10.8
236	0.295	1.81	302	0.00228	11.2
238	0.258	1.93	304	0.00192	11.7
240	0.226	2.06	306	0.00162	12.2
242	0.198	2.20	308	0.00136	12.6
244	0.174	2.35	310	0.00114	13.2
246	0.153	2.51	312	0.000962	13.6
248	0.135	2.68	314	0.000835	14.2
250	0.119	2.86	316	0.000689	14.7
252	0.105	3.05	318	0.000571	15.2
254	0.0927	3.25	320	0.000491	15.8
256	0.0823	3.47	322	0.000443	16.3
258	0.0728	3.69	324	0.000354	16.9
260	0.0644	3.92	326	0.000282	17.5
262	0.0566	4.17	328	0.000242	18.1
264	0.0496	4.42	330	0.000206	18.7
266	0.0435	4.69	332	0.000174	19.3
268	0.0380	4.96	334	0.000146	19.9
270	0.0331	5.25	336	0.000107	20.5
272	0.0287	5.54	338	0.000090	21.2
274	0.0248	5.85	340	0.000066	21.8

[a] Units of 10^{-18} cm^2 $molecule^{-1}$. [b] Units of 10^{-3} K^{-1}.

via a least-squares fits to determine $B(\lambda)$. This empirical parametrization method was also used in our previous study of the PAN UV absorption spectrum.[9] The room-temperature PPN cross sections and the $B(\lambda)$ values derived from the fits are listed in Table 1 at 2 nm increments over the wavelength range 210−340 nm. The calculated spectra reproduce the measured spectra well within the measurement precision (see below).

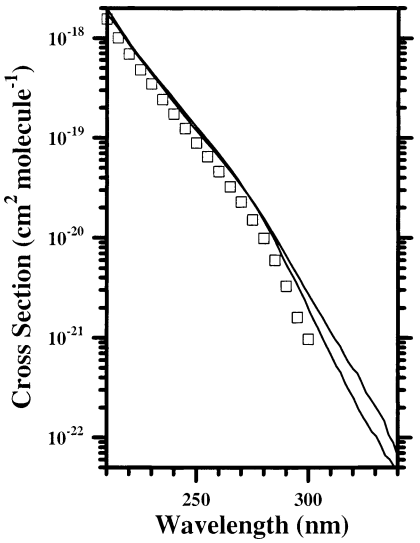

Figure 2. Comparison of the PPN ($CH_3CH_2C(O)OONO_2$) cross sections measured in this work (solid line) with those reported by Senum et al.[14] (squares). The quoted uncertainty in the Senum et al. data is ~10% at all wavelengths. The estimated (2σ) uncertainty in the PPN cross sections from this work at 248 and 308 nm are 10 and 15%, respectively (see text). For comparison, we have also shown the PAN ($CH_3C(O)OONO_2$) spectrum (lower line) reported by Talukdar et al.[9]

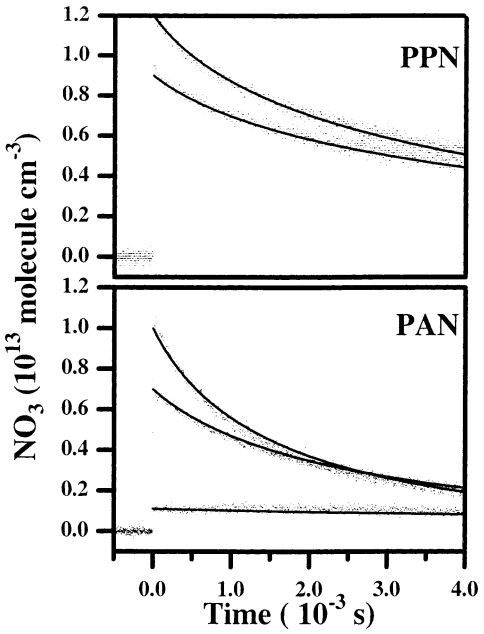

Figure 3. NO_3 temporal profiles measured following the 248 nm photolysis of PAN ($CH_3C(O)OONO_2$) and PPN ($CH_3CH_2C(O)OONO_2$) (dots) in 520 Torr N_2. The solid lines were calculated using the chemical reaction mechanism described in the text.

The uncertainty in the PPN cross sections is determined by the accuracy of the measurement (±0.0003 absorbance units), the absorption cell path length (± 0.5 cm), accuracy of the NO_2 spectral subtraction (wavelength dependent), and the purity of the PPN sample (>95%). UV and infrared reference spectra of the most likely organic impurities in the PPN synthesis, propionic anhydride and propionic acid, were recorded. Both molecules are relatively weak UV absorbers. On the bases of the simultaneous UV and infrared measurements of the PPN sample, spectral interference in the UV from these compounds was below our detection limit. The purity of the PPN sample was estimated from measurements of NO_y impurities using the methods described by Williams et al.[20] and the above measurements of the main organic impurities, the anhydride and the acid. The 2σ uncertainties (95% confidence level) in the PPN cross sections are estimated to be 10% at 210 nm, 10% at 248 nm, and 15% at 308 nm.

Only Senum et al.[14] have previously reported UV absorption cross sections of PPN. In their study, UV spectra were recorded using a scanning monochromator and absolute pressure measurements were used to determine the absorption cross sections for PPN. Their PPN cross section data are shown in Figure 2 for comparison with the values determined in this study. Our PPN cross section values are systematically larger than those of Senum et al. throughout the entire wavelength range common to both studies. The difference in cross section is ~25% at 250 nm and becomes even larger at longer wavelengths. The long wavelength region of the absorption spectrum is the most difficult to measure accurately due to the NO_2 spectral interference and the small cross section values. Therefore, it is not surprising that this region shows the largest disagreements. The same systematic difference in cross section values was found in our previous studies of PAN[9] when compared with the PAN absorption cross sections reported by Senum et al.[14] in the same study.

The PPN spectrum is continuous over the entire wavelength range and closely resembles the shape of the PAN spectrum at wavelengths less than 280 nm. At longer wavelengths the PPN cross sections are systematically larger than those of PAN (see Figure 2). These systematic differences in absorption spectra with increasing carbon chain length have also been observed for the alkyl nitrates, comparing methyl to ethyl nitrate.[2,21]

TABLE 2: Summary of NO_3 Quantum Yield Measurements

	248 nm		308 nm	
molecule	σ(248 nm)	$\Phi_\lambda(NO_3)$	σ(308 nm)	$\Phi_\lambda(NO_3)$
PAN	1.46×10^{-19}	0.19 ± 0.04^a	8.16×10^{-22}	0.41 ± 0.10
PPN	1.36×10^{-19}	0.22 ± 0.04	1.38×10^{-21}	0.39 ± 0.04
N_2O_5	4.19×10^{-19}	0.80	2.4×10^{-20}	1.0

[a] Uncertainties are 2σ of the measurement precision.

NO_3 Quantum Yield Measurements. Representative NO_3 temporal profiles measured following the pulsed photolysis of PAN and PPN at 248 nm are shown in Figure 3. The NO_3 concentration is highest immediately following the photolysis pulse and decayed over the next 4 ms of the measurement. The NO_3 decay rate was observed to be dependent on the concentration and identity of photolysis products as described below. The NO_3 profiles recorded following photolysis of PAN and PPN at 308 nm showed no measurable decay, $<10\ s^{-1}$, due to the low initial NO_3 concentrations. For quantum yield calculations, eq 4, the NO_3 signal measured immediately following the photolysis pulse was used.

The NO_3 quantum yield results are summarized in Table 2. The quoted quantum yield values are the average of 10 independent determinations where the uncertainties are 2 standard deviations. The absorption cross sections and N_2O_5 photolysis quantum yields used in the data analysis, eq 4, are also given in Table 2. The NO_3 quantum yields for PAN and PPN have nearly identical values; $\Phi_{248}^{NO_3}(X)$ values of 0.19 and 0.22 and $\Phi_{308}^{NO_3}(X)$ values of 0.41 and 0.39 were determined for PAN and PPN, respectively. These measurements show that the NO_3 yield increases, approximately a factor of 2, from 248 to 308 nm. Therefore, in the wavelength range most important for photolysis of these compounds in the atmosphere, 305−330 nm, the NO_3 yield in the photolysis is significant.

Our NO_3 quantum yield value for PAN photolysis at 248 nm can be compared with the value recently reported by Mazely et

al.[13] Mazely et al.[12,13] detected NO_2 and NO_3 photofragments following PAN photolysis at 248 nm using laser-induced fluorescence detection at total pressures <10 Torr. Their measurements were quantified relative to HNO_3 photolysis for NO_2 and N_2O_5 photolysis for NO_3. These measurements show the quantum yield for PAN photolysis at 248 nm to be near unity with a significant yield of NO_3. They report $\Phi_{248}^{NO_3}(PAN) = 0.3 \pm 0.1$ while using $\Phi_{248}^{NO_3}(N_2O_5) = 1$ in the data analysis. The quoted uncertainty is 2σ of their measurement precision. Recent studies from our laboratory[18] have determined the NO_3 yield for N_2O_5 photolysis at 248 nm to be less than one. Using the results from Harwood et al. and consideration of other previous measurements[22] leads to a value of $\Phi_{248}^{NO_3}(N_2O_5) = 0.80 \pm 0.1$. Scaling the Mazely et al. NO_3 yield to this value of $\Phi_{248}^{NO_3}(N_2O_5)$ produces $\Phi_{248}^{NO_3}(PAN) = 0.38$, which yields excellent agreement between the two NO_3 quantum yield values for 248 nm photolysis of PAN.

NO_2 and NO_3 can be produced through several photolysis channels in PAN photolysis (see Mazely et al.[13] for discussion). The measurement of photolysis fragments other than NO_2 and NO_3, in particular O atoms, would help identify the relative significance of these various channels. Currently the difference between NO_2 and NO_3 production is thought to be of only minor consequence in atmospheric chemistry (see discussion below).[6,13] There are no PPN photolysis product studies reported in the literature with which to compare our measurements.

NO_3 Decay Analysis. The measured NO_3 decays following 248 nm photolysis of PAN and PPN show significant decay rates under certain conditions. We have evaluated these temporal profiles, in the section below, to evaluate if the observed NO_3 decays are reproduced with the expected radical chemistry and rate coefficients. First, the upper limit for the NO_3 first-order loss rate observed following the 308 nm photolysis of PAN and PPN was $<10\ s^{-1}$. This places an upper limit on the rate coefficient for the reaction of NO_3 with PAN and PPN

$$NO_3 + PAN/PPN \rightarrow \text{products} \qquad (5')$$

of 2×10^{-16} cm^3 molecule^{-1} s^{-1}. These measurements also provide a limit on the first-order loss of NO_3 due to reaction with the NO_2 impurity via

$$NO_2 + NO_3 + M \leftrightarrow N_2O_5 + M \qquad (6)$$

and show that reaction 6 does not make a significant contribution to the observed decay. (The NO_2 impurity level is greater than the NO_2 produced in the 248 nm photolysis experiments.) The NO_3 decays following 248 nm photolysis, Figure 3, are nonexponential and the rates are dependent on the initial radical concentration. Also, the NO_3 decay rates following PPN photolysis are slower than observed with PAN at the same initial NO_3 concentration. To understand the NO_3 decays, we have numerically simulated the NO_3 profiles (heavy lines in Figure 3) assuming (1) only the $CH_3C(O)OO + NO_2$ and $CH_3C(O)O + NO_3$ channels for PAN photolysis and only the $CH_3CH_2C(O)OO + NO_2$ and $CH_3CH_2C(O)O + NO_3$ channels for PPN photolysis are active and (2) $\Phi_\lambda^{NO_3}(PAN \text{ or } PPN) = 0.2$.

Under our experimental conditions both the $CH_3C(O)O$ and $CH_3CH_2C(O)O$ radicals rapidly decompose

$$CH_3C(O)O \rightarrow CH_3 + CO_2 \qquad (7)$$

and

$$CH_3CH_2C(O)O \rightarrow CH_3CH_2 + CO_2 \qquad (8)$$

Rate coefficients for the reactions

$$CH_3C(O)OO + NO_3 \rightarrow CH_3 + CO_2 + O_2 + NO_2 \qquad (9)$$

$$CH_3 + NO_3 \rightarrow CH_3O + NO_2 \qquad (10)$$

$$CH_3CH_2C(O)OO + NO_3 \rightarrow CH_3CH_2 + CO_2 + O_2 + NO_2 \qquad (11)$$

and

$$CH_3CH_2 + NO_3 \rightarrow CH_3CH_2O + NO_2 \qquad (12)$$

have not been reported in the literature and were varied in the simulations. Other rate coefficients used in the simulation were taken from DeMore et al.[22] The calculated NO_3 profiles shown in Figure 3, solid lines, were obtained with $k_9 = 1.7 \times 10^{-11}$, $k_{10} = 5 \times 10^{-12}$, $k_{11} = 8 \times 10^{-12}$, and $k_{12} < 1 \times 10^{-12}$ (all in units of cm^3 molecule^{-1} s^{-1}). These rate coefficients are not uniquely determined from such a limited data set but have reasonable values when compared with previously measured NO_3 rate coefficients with alkylperoxy and alkoxy radicals.[22] Therefore, the observed NO_3 decays can be interpreted using the expected chemistry and reasonable rate coefficient data.

Atmospheric Implications. Most numerical models of NO_x-HC chemistry that have included PAN and PPN have focused on the polluted lower troposphere. Models of global tropospheric chemistry have simulated PAN concentrations, but only a few have attempted to simulate PPN as well.[23,24] Identical loss rates are assumed for PAN and PPN due to thermal decomposition, based on laboratory studies that show them to be the same within experimental uncertainties.[25] Photolytic loss of PAN and PPN are often assumed to be the same or are estimated from the data of Senum et al.[14] which actually results in a slightly slower rate for PPN photolysis. Products of PAN and PPN photolysis have been assumed to be the peroxyacetyl (PA) radical + NO_2.

There are two important points relating to the PPN UV absorption cross sections to be noted. First, the atmospheric photolysis rate of PPN calculated using the UV absorption cross sections determined in this study will be significantly larger than that reported by Senum et al.[14] Figure 2 shows the PPN absorption cross section data measured in this and that taken from Senum et al.[14] Photolysis rates will be a factor of 10 larger using the present cross section values. Second, the atmospheric photolysis rate calculated for PPN is also significantly different than that of PAN. The red shift of the PPN spectrum relative to PAN significantly increases the atmospheric photolysis rate of PPN relative to PAN. For example, the photolysis rate of PPN at 40° N in the summer time at 17 km is about twice that of PAN. Therefore, PPN is less efficient than PAN for long-range transport of NO_x and treating them the same in atmospheric model calculations would lead to systematic errors. Concentrations of PPN relative to PAN have been measured mostly in the polluted continental troposphere, with only a few observations in the remote atmosphere. Anthropogenic NO_x-HC chemistry appears to produce PPN/PAN ratios on the order of 12−20%,[2,8] while biogenic hydrocarbon production of PAN can shift the ratio to lower values. Observations in the remote troposphere show values of a few percent or below.[26−28] While a number of factors must be considered, e.g., the availability of precursors in the remote troposphere, these observations are consistent with a faster photolysis rate for PPN relative to PAN.

The atmospheric significance of the PAN quantum yield measurements was evaluated with a photochemical box model including a detailed tropospheric HO_x-NO_x-hydrocarbon

mechanism.[29] The model was initialized with median background upper tropospheric (8−12 km) observations from the subsonic assessment ozone and nitrogen oxide experiment (SONEX)[30] and an altitude of 10 km. Each modeled compound's time evolution was affected by only photochemical reactions; no physical or dynamical processes, with the exception of aerosol uptake of NO_3 and N_2O_5, were considered. PAN photolysis rates were calculated with a radiative transfer model[31] using the temperature-dependent absorption cross sections of Talukdar et al.[9] extrapolated to the temperature of the input data (227 K). Other relevant rate coefficients were taken from DeMore et al.[22] The quantum yield of the NO_3 photolysis channel of PAN, reaction 2b, ϕ_{NO_3}, was assumed to be wavelength-independent. Three model cases were run: $\phi_{NO_3} = 0$ (control case reflecting the current assumption in most photochemical models), $\phi_{NO_3} = 0.4$ (from the measurements of this work), and $\phi_{NO_3} = 1.0$ (upper limit). We compared the nonzero ϕ_{NO_3} cases to the control case to evaluate the relative impact on PAN lifetime and on the levels of various compounds.

The effective PAN lifetime is defined here as the inverse of the total first-order rate of all reactions which lead to an actual loss of PAN. Thermal decomposition, reaction −1, and photolysis via the NO_2 channel, reaction 2a, represent PAN sinks if the resulting peroxyacetyl (PA, $CH_3C(O)OO$) radical reacts with NO, HO_2, CH_3O_2, or itself instead of with NO_2. NO was the most important PA reactant during daytime for the SONEX data ($NO/NO_2 = 4$ at noon), while NO_2 dominated at night. The modeled fraction of PA irretrievably lost varied between 90% during midday and less than 1% at night. The other PAN loss channels, photolysis via NO_3, reaction 2b, and reaction with OH, always result in a loss of PA. The calculated effective PAN lifetime was about 4 months (diurnally averaged) for the SONEX conditions. After including reaction 2b, PAN lifetimes were reduced by 5−10% during midday and by up to 50% just after sunrise and before sunset. The diurnally averaged decrease in the PAN lifetime was 3% for $\phi_{NO_3} = 0.4$ and about 6% for $\phi_{NO_3} = 1.0$.

PAN is a large reservoir of NO_x in the upper troposphere: median background levels of PAN and NO_x in SONEX were 64 and 93 pptv, respectively. NO_3 resulting from PAN photolysis could produce up to two molecules of odd-oxygen rather than the one O_x derived from NO_2. Even small changes in the lifetime of PAN and in its photolysis products could therefore potentially impact the budgets of NO_x and O_3 in the upper troposphere. However, even the upper limit case of $\phi_{NO_3} = 1.0$ resulted in only small changes to the modeled chemical distribution. Relative to the $\phi_{NO_3} = 0$ case, after 2 weeks of reaction PA had decreased by 5% (diurnally averaged), while PAN, NO_x, and HO_x levels changed by at most 2% and O_3 increased by <0.1%. These small changes in the chemical distribution reflect the long lifetime of PAN at this altitude. NO_x release from PAN is generally too slow to significantly affect O_3 distributions in the upper troposphere, compared with other NO_x sources, such as lightning and aircraft emissions, or with mixing of air masses enriched in NO_x and/or O_3 via convection from the boundary layer or stratosphere−troposphere exchange.

Peroxyacetyl radicals can participate in the formation of peroxyacetic acid and acetic acid, through reaction with HO_2.[32,33] The results of this work imply that the calculated upper atmospheric source of these compounds would be reduced. While the analogous chemistry for peroxypropionyl radicals has not been studied as thoroughly, a significant photolysis channel producing $CH_3CH_2C(O)O$ radical will also effect subsequent HO_2 chemistry.

In the lower troposphere, thermal decomposition is the dominant PAN sink and the impact of changes to the photolysis channels are not significant. In the stratosphere, the NO/NO_2 ratio is smaller and PAN reformation via reaction 1 is more favorable than in the upper troposphere. We estimate that accounting for the NO_3 photolysis channel would decrease the PAN lifetime in the lower stratosphere by as much as 20%.

References and Notes

(1) Singh, H. B. *Environ. Sci. Technol.* **1987**, *21*, 320.

(2) Roberts, J. M. *Atmos. Environ.* **1990**, *24A*, 243.

(3) Altshuller, A. P. *J. Air Waste Manage. Assoc.* **1993**, *43*, 1221.

(4) Parrish, D. D.; Buhr, M. P.; Trainer, M.; Norton, R. B.; Shimshock, J. P.; Fehsenfeld, F. C.; Anlauf, K. G.; Bottenheim, J. W.; Tang, Y. Z.; Wiebe, H. A.; Roberts, J. M.; Tanner, R. L.; Newman, L.; Bowersox, V. C.; Olszyna, K. J.; Bailey, E. M.; Rodgers, M. O.; Wang, T.; Berresheim, H., Roychowdhury, U.K.; Demerjian, K. L. *J. Geophys. Res.* **1993**, *98*, 2927.

(5) Singh. H. B.; Herlth, D.; O'Hara, D.; Zahnle, K.; Bradshaw, J. D.; Sandholm, S. T.; Talbot, R.; Gregory, G. L.; Sachse, G. W.; Blake, D. R.; Wofsy, S. C. *J. Geophys. Res.* **1994**, *99*, 1821.

(6) Moxim, W. J.; Levy, H., II; Kasibhatla, P. S. *J. Geophys. Res.* **1996**, *101*, 12621.

(7) Brühl C.; Pöschl, U.; Crutzen, P. J.; Steil, B. *Atmos. Environ.* **2000**, *34*, 3931.

(8) Roberts, J. M.; Williams, J.; Baumann, K.; Buhr, M. P.; Goldan, P. D.; Holloway, J.; Hubler, G.; Kuster, W. C.; McKeen, S. A.; Ryerson, T. B.; Trainer, M.; Williams, E. J.; Fehsenfeld, F. C.; Bertman, S. B.; Nouaime, G.; Seaver, C.; Grodzinsky, G.; Rodgers, M.; Young, V. L. *J. Geophys. Res.* **1998**, *103*, 22473.

(9) Talukdar, R. K.; Burkholder, J. B.; Schmoltner, A.-M.; Roberts, J. M.; Wilson, R.; Ravishankara, A. R. *J. Geophys. Res.* **1995**, *100*, 14163.

(10) Villalta, P. W.; Lovejoy, E. R.; Hanson, D. R. *Geophys. Res. Lett.* **1996**, *23*, 1765.

(11) Williams, J.; Roberts, J. M.; Fehsenfeld, F. C.; Bertman, S. B.; Buhr, M. P.; Goldan, P. D.; Hübler, G.; Kuster, W. C.; Ryerson, T. B.; Trainer, M.; Young, V. *Geophys. Res. Lett.* **1997**, *24*, 1099.

(12) Mazely, T. L.; Friedl, R. R.; Sander, S. P. *J. Phys. Chem.* **1995**, *99*, 8162.

(13) Mazely, T. L.; Friedl, R. R.; Sander, S. P. *J. Phys. Chem. A* **1997**, *101*, 7090.

(14) Senum, G. I.; Lee, Y.-N.; Gaffney, J. S. *J. Phys. Chem.* **1984**, *88*, 1269.

(15) Stephens, E. R. *Anal. Chem.* **1964**, *26*, 928.

(16) Tsalkani, N.; Toupance, G. *Atms. Environ.* **1989**, *23*, 1849.

(17) Yokelson, R. J.; Burkholder, J. B.; Fox, R. W.; Ravishankara, A. R. *J. Phys. Chem. A* **1997**, *101*, 6667.

(18) Harwood: M. H.; Burkholder, J. B.; Ravishankara, A. R. *J. Phys. Chem. A* **1998**, *102*, 1309.

(19) Yokelson, R. J.; Burkholder, J. B.; Fox, R. W.; Talukdar, R. K.; Ravishankara, A. R. *J. Phys. Chem.* **1994**, *98*, 13144.

(20) Williams, J.; Roberts, J. M.; Bertman, S. B.; Stroud, C. A.; Fehsenfeld, F. C.; Baumann, K.; Buhr, M. P.; Knapp, K.; Murphy, P. C.; Nowick, M.; Williams, E. J. *J. Geophys. Res.* **2000**, *105*, 28943.

(21) Talukdar, R. K.; Burkholder, J. B.; Hunter, M.; Gilles, M. K.; Roberts, J. M.; Ravishankara, A. R. *J. Chem. Soc., Faraday Trans.* **1997**, *93*, 2797.

(22) DeMore, W. B.; Sander, S. P.; Golden, D. M.; Hampson, R. F.; Kurylo, M. J.; Howard, C. J.; Ravishankara, A. R.; Kolb, C. E.; Molina, M. J. Chemical Kinetics and Photochemical Data for Use in Stratospheric Modeling. Evaluation 12, JPL Publication 97−4; Jet Propulsion Laboratory: Pasadena, 1997.

(23) Kasting, J. F.; Singh, H. B. *J. Geophys Res.* **1986**, *91*, 13239.

(24) Singh, H. B.; Kasting, J. F. *J. Atmos. Chem.* **1988**, *7*, 261.

(25) Kirchner, F.; Mayer-Figge, A.; Zabel, F.; Becker, K. H. *Int. J. Chem. Kinet.* **1999**, *31*, 127.

(26) Singh, H. B.; Salas L. J. *Atmos. Environ.* **1989**, *23*, 231.

(27) Ridley, B. A.; Shetter, J. D.; Walega, J. G.; Madronich, S.; Elsworth, C. M.; Grahek, F. E.; Fehsenfeld, F. C.; Norton, R. B.; Parrish, D. D.; Hübler, G. H.; Buhr, M.; Williams, E. J.; Allwine, E. J.; Westberg, H. H. *J. Geophys. Res.* **1990**, *95*, 13949.

(28) Walega, J. G.; Ridley, B. A.; Madronich, S.; Grahek, F. E.; Shetter, J. D.; Sauvain, T. D.; Hahn, C. J.; Merrill, J. T.; Bodhaine, B. A.; Robinson, E. *J. Geophys. Res.* **1992**, *97*, 10311.

(29) Frost, G. J.; Trainer, M.; Allwine, G.; Buhr, M. P.; Calvert, J. G.; Cantrell, C. A.; Fehsenfeld, F. C.; Goldan, P. D.; Herwehe, J.; Hubler, G.;

Kuster, W. C.; Martin, R.; McMillen, R. T.; Montzka, S. A.; Norton, R. B.; Parrish, D. D.; Ridley, B. A.; Shetter, R. E.; Walega, J. G.; Watkins, B. A.; Westberg, H. H.; Williams, E. J. *J. Geophys. Res.* **1998**, *103*, 22491.

(30) Jaeglé, L.; Jacob, D. J.; Brune, W. H.; Faloona, I.; Tan, D.; Heikes, B. G.; Kondo, Y.; Sachse, G. W.; Anderson, B.; Gregory, G. L.; Singh, H. B.; Pueschel, R.; Ferry, G.; Blake, D. R.; Shetter, R. E. *J. Geophys. Res.* **2000**, *105*, 3877.

(31) Madronich, S. J.; Zeng, J.; Stamnes, K. http://www.acd.ucar.edu/TUV/. 1998.

(32) Tyndall, G. S.; Cox; R. A.; Granier, C.; Lesclaux, R.; Moortgat, G. K.; Pilling, M. J.; Ravishankara, A. R.; Wallington, T. J. *J. Geophys. Res.* **2001**, *106*, 12, 157.

(33) Tomas, A.; Villenave, E.; Lesclaux, R. *J. Phys. Chem. A.* **2001**, *105*, 3505.